Water Resources Research

RESEARCH ARTICLE
10.1029/2023WR034699

Quantifying the Impact of Spatiotemporal Resolution on the Interpretation of Fluvial Geomorphic Feature Dynamics From Sentinel 2 Imagery: An Application on a Braided River Reach in Northern Italy

Elisa Bozzolan[1,2], Andrea Brenna[1], Nicola Surian[1], Patrice Carbonneau[3], and Simone Bizzi[1]

[1]Department of Geosciences, Università degli Studi di Padova, Padova, Italy, [2]Cabot Institute, University of Bristol, Bristol, UK, [3]Department of Geography, Durham University, Durham, UK

Key Points:

- The spatial (10 m) and temporal (5 days) resolution of Sentinel 2 (S2) images define the river geomorphic change that we can detect
- A comparison with other spatiotemporal resolutions shows that the S2-derived active channel trajectory is robust despite the spatial error
- Low spatial, but high temporal resolution data can be more informative on river geomorphic processes than multiannual images at centimetric resolution

Correspondence to:
E. Bozzolan,
elisa.bozzolan@unipd.it

Citation:
Bozzolan, E., Brenna, A., Surian, N., Carbonneau, P., & Bizzi, S. (2023). Quantifying the impact of spatiotemporal resolution on the interpretation of fluvial geomorphic feature dynamics from Sentinel 2 imagery: An application on a braided river reach in Northern Italy. *Water Resources Research*, *59*, e2023WR034699. https://doi.org/10.1029/2023WR034699

Received 17 FEB 2023
Accepted 31 OCT 2023

Author Contributions:
Conceptualization: Elisa Bozzolan, Andrea Brenna, Nicola Surian, Simone Bizzi
Data curation: Elisa Bozzolan, Andrea Brenna
Funding acquisition: Simone Bizzi
Investigation: Elisa Bozzolan
Methodology: Elisa Bozzolan, Andrea Brenna, Simone Bizzi
Software: Patrice Carbonneau
Visualization: Elisa Bozzolan
Writing – original draft: Elisa Bozzolan, Andrea Brenna

Abstract Machine learning algorithms applied on the publicly available Sentinel 2 images (S2) are opening the opportunity to automatically classify and monitor fluvial geomorphic feature (such as sediment bars or water channels) dynamics across scales. However, there are few analyses on the relative importance of S2 spatial versus temporal resolution in the context of geomorphic research. In a dynamic, braided reach of the Sesia River (Northern Italy), we thus analyzed how the inherent uncertainty associated with S2's spatial resolution (10 m pixel size) can impact the significance of the active channel (a combination of sediment and water) delineation, and how the S2's weekly temporal resolution can influence the interpretation of its evolutionary trajectory. A comparison with manually classified images at higher spatial resolutions (Planet: 3 m and orthophoto: 0.3 m) shows that the automatically classified water is ~20% underestimated whereas sediments are ~30% overestimated. These classification errors are smaller than the geomorphic changes detected in the 5 years analyzed, so the derived active channel trajectory can be considered robust. The comparison across resolutions also highlights that the yearly Planet- and S2-derived active channel trajectory are analogous and they are both more effective in capturing the river geomorphic response after major flood events than the trajectory derived from sequential multiannual orthophotos. More analyses of this type, across different types of river could give insights on the transferability of the spatial uncertainty boundaries found as well as on the spatial and temporal resolution trade-off needed for supporting different geomorphic analyses.

1. Introduction

River corridors encompass wet channels, exposed deposits such as sediment bars, riparian zones, and floodplains potentially covered by vegetation (Harvey & Gooseff, 2015). These fluvial geomorphic features can gradually and/or abruptly change over time. Monitoring such transformations (e.g., their lateral migration or the dynamic change of the channel widths—e.g., Dean & Schmidt, 2013; Stecca et al., 2019) provide the basis for a better understanding of the underlying river processes, natural and anthropogenic drivers of the river morphological changes, as well as channel adjustment times (Brierley et al., 2010; Rinaldi et al., 2017). This information is key to infer future conditions of the river corridor and eventually support its restoration and management (Brierley & Fryirs, 2016; Grabowski et al., 2014).

In this context, airborne and spaceborne remote sensing data has become a crucial tool (e.g., Bizzi et al., 2019; Righini & Surian, 2018; Tomsett & Leyland, 2019). Sub-metric resolution images have often been analyzed to detect fluvial geomorphic features, arguing that high resolution images can better support the translation of river geomorphic changes into process-understanding (Carbonneau et al., 2012; Rivas Casado et al., 2016). Unfortunately, these images (such as orthophotos or unpiloted image acquisitions) when publicly available at catchment or regional scale are generally associated with a low temporal resolution, such as years or decades (e.g., http://www.pcn.minambiente.it/mattm/). In these time windows, images become "snapshots" that can reveal gross change in river planform and lateral erosion rates but mask the episodic nature of the channel response in its transient states (Petts & Gurnell, 2005), which can in turn help the interpretation of longer-term trajectories (Piégay et al., 2020; Ziliani & Surian, 2012). To better decipher river morphodynamic processes, it is therefore critical to monitor both rapid and abrupt river changes (e.g., channel widening induced by an extreme hydrological event) as well as progressive and incremental changes (e.g., bank erosion normally occurring on the external part of a channel bend), that often interplay in the river systems (Boothroyd et al., 2021).

Writing – review & editing: Elisa Bozzolan, Andrea Brenna, Nicola Surian, Patrice Carbonneau, Simone Bizzi

The publicly available, multi-spectral Copernicus Sentinel-2 (S2) data has the potential to meet this challenge. S2 images were first acquired in 2016 with a temporal resolution of 5 days (cloud coverage permitting) and a spatial resolution of maximum 10 m. Their wide (global) spatial coverage (same as the Landsats 7 and 8) is slowly (Piégay et al., 2020) opening the opportunity to test current geomorphological theories across scales, times and locations (Brierley et al., 2013). However, understanding what spatial and temporal resolution could be most effective to solve specific geomorphic research questions is still an open issue (Piégay et al., 2020). There is a relation between the type of analysis (e.g., gross or fine morphological changes), type of river, and spatiotemporal resolution adopted. For example, slow geomorphic changes of small rivers could be captured by high spatial resolutions and long revisit intervals, whereas the geomorphic changes of highly dynamic rivers might be visible on coarser spatial resolutions but would require high revisit times.

In general, temporal errors will be intimately associated with the process under analysis, its rate of change and the time between consequent image acquisition (Ziliani & Surian, 2012). Spatial errors will instead depend on the relation between the river size, river complexity and the image spatial resolution (Gilvear & Bryant, 2016; Rowland et al., 2016). Even in wide river channels, satellite imagery pixels edges do not coincide with the edges of the objects on the ground; pixels will contain a number of classes (mixed pixels) that include for example, sediment, water and vegetation. If these mixed pixels are classified with one class (e.g., water), it means that the other classes (e.g., sediment or vegetation) within those pixels will get unavoidably underestimated. The lower the spatial resolution, the more relevant this issue becomes, raising questions on the real extent of the fluvial geomorphic features measured or on the true geomorphic temporal change that can be detected (Donovan et al., 2019; Ling et al., 2019). We could therefore ask: given that the delineation of the geomorphic features is uncertain due to the spatial resolution, how much can we trust the S2 images for the interpretation of their dynamics and trajectories? And how does such interpretation compare to the understanding that can be derived from the analysis of few (e.g., one each year), manually classified submeter spatial resolution images, as commonly done in geomorphological studies (e.g., Brenna et al., 2021; Kondolf et al., 2007; Ziliani & Surian, 2012)?

We addressed these questions on a reach of the Sesia River—a dynamic braided river in the North-West of Italy. We first compare the classes of water, sediment, and vegetation automatically classified on the S2 images with those manually classified in the available orthophotos (0.3 m resolution). This comparison allowed the quantification of the spatial error. Then, for the first time, we evaluated how such a spatial uncertainty could influence the interpretation of the S2-derived active channel (defined as the sum of the water and sediment areas) trajectory. To better discriminate the classification (automatic vs. manual) errors from the spatiotemporal resolution errors, we also included in the analysis a yearly, manually classified Planet image (3 m resolution).

The analysis across different spatiotemporal resolutions determined: (a) the type of error derived from the planet-orthophoto comparison, associated with a manual classification and an increased spatial (from 0.3 to 3 m) and temporal resolution (from multi-year to yearly); (b) the type of error derived from the S2-orthophoto comparison, associated with an automatic classification of the S2 images versus the manual classification of the orthophoto, a coarser spatial resolution (from 0.3 to 10 m) and a finer temporal resolution (from multi-year to weekly); (c) how these errors compared between the type of classifiers and spatial resolutions, assessing the associated challenges and opportunities of analyzing river evolutionary trajectories in terms of fluvial dynamics, processes and drivers, at various temporal resolutions.

2. Study Site

The Sesia River catchment is located in the North-West Italy and cover a total area of 3,038 km^2 with an elevation ranging from 4,464 to 96 m a.s.l (Figure 1). The Sesia River is a northern tributary of the Po River and has a total length of 140 km. The upper part of its course is within the western Alps. Starting from Romagnano Sesia, the river flows with North-South direction into the High Po Plain, developing a wide and dynamic channel with transitional or multi-thread planform configuration. Downstream from Vercelli, the channel configuration changes into single-thread with sinuous or meandering morphology up to the confluence with the Po River. The mean annual rainfall in the catchment is 1,013 mm and the mean annual discharge at Palestro is about 70 $m^3\ s^{-1}$ (Scorpio & Piégay, 2021).

In this work, we focused on a 3.7 km-long reach of the Sesia River located in the High Po Plain between Carpignano Sesia and Arborio, where the river displays a wandering to braided configuration with an active channel

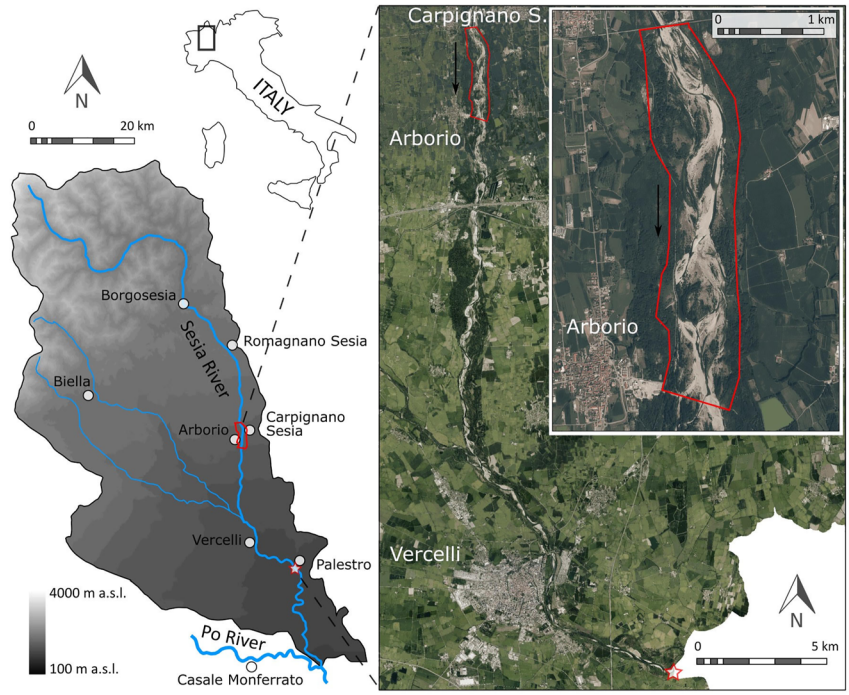

Figure 1. Location map of the Sesia River catchment and an extract of the Sesia River from the orthophoto 2018. The area of analysis which will be classified into classes of water, sediment and vegetation is highlighted with the red polygon (zoomed in on the top right-hand side panel). The red star identifies the Palestro gauging station where the hydrometric levels are recorded by the Agenzia Interregionale per il Fiume Po. The station is about 30 km downstream the analyzed river sector. Black arrows indicate flow direction.

width of 200–400 m (Figure 1). Beside the active channel *stricto sensu* (i.e., the area occupied by low flow channels and sediment bars; Liébault & Piégay, 2002), our investigation also considered the within-channel vegetated islands and the surrounding riparian areas (red polygon in Figure 1). The total area of analysis has an extension of about 2.6 km^2.

The time window of investigation extended from January 2018 to December 2022 (5 years). On the second of October 2020, an exceptional meteorological event accompanied with intense and prolonged rainfall lasting for 24 hr with cumulative precipitation of about 450 mm affected North-West Italy, causing high-magnitude flooding in the Sesia River (De Petris et al., 2021). The maximum water discharges estimated at the sections of Borgosesia and Palestro were of about 3,000 and 5,000 $m^{-3}s^{-1}$, respectively, that is, values associated with recurrence intervals higher than 100 years (ARPA, 2020).

3. Materials and Methods

This work aims to compare the automatic classification of the water, sediment and vegetation classes performed on S2 images with the manual discrimination of the same classes performed on satellite images and aerial orthophotos at higher spatial resolutions (3 and 0.3 m, respectively). These classes and their evolution are assumed to represent respectively the fluvial geomorphic features (e.g., exposed sediment bars) and their dynamics (e.g., a decrease in their area). The fluvial geomorphic feature dynamics over the considered 5 years instead define the river evolutionary trajectory (e.g., whether the active channel is widening or narrowing).

From now on, the term "S2" will refer to the S2-based automatic classification and the terms "Planet" and "orthophoto" will refer to the Planet-, and orthophoto-based manual classifications, respectively.

3.1. Image Selection

We considered a period between January 2018 and December 2022, for which both the Planet and the atmospherically corrected S2 images are available throughout the whole year. In this time window, we found only two

Table 1
Type of Images Used in This Work, Their Spatial Resolution and the Classification Approach Adopted

	2018	2019	2020	2021	2022	Resolution-classification
Orthophoto	1 (19/08/2018)	0	0	0	1 (12/05/2022)	0.3 m-manual
Planet	1 (19/08/2018)	1 (28/06/2019)	1 (23/06/2020)	1 (14/06/2021)	1 (10/05/2022)	3 m-manual
Sentinel 2	15 (20/08/2018)	22	25	23	25 (11/05/2022)	10 m-automatic

Note. The date of acquisition is reported only for those images that were used for the pixel-by-pixel comparison (see Section 3.2).

orthophotos (spatial resolution: 0.3 m) of the study site, taken in the summer 2018 and spring 2022. These two images were acquired by AGEA (Agenzia per le erogazioni in agricoltura) and by the Authority of the Po Basin, respectively (see the links reported in the data availability statement). For the spatial comparison, we then downloaded the Planet (https://www.planet.com/) and the Sentinel Level-2A (https://scihub.copernicus.eu) images on the same dates (or on the closest available date—see Table 1 where the acquisition dates are reported within brackets). For the temporal comparison instead, we downloaded one Planet image per year and all the S2 images available with a cloud coverage below 5% (110 images in total).

The Planet Level-3B images (Harmonised Analytic Ortho Scene) from the Planet CubeSat constellation have four radiometric bands (Red-Green-Blue and the near infrared) with spatial resolution of 3 m. These images are commercially available daily at nadir since 2017 for the study site. They were downloaded with radiometric-, sensor-, and geometric-correction (including the atmospheric correction). The Sentinel-2A images (S2) from the European Copernicus mission have in total 12 radiometric bands, four of which are natively acquired at 10 m resolution (Red-Green-Blue and the near infrared). These images are freely available weekly since mid-2017 and they were downloaded already atmospherically corrected and orthorectified.

3.2. Fluvial Geomorphic Feature Delineation and Accuracy Assessment

All the image sources were clipped within the polygon of the area of interest (Figure 1). Using a geographic information system, the orthophotos and the Planet images (visualized in false-color) were manually classified over the area of analysis into water, sediment and vegetation based on visual interpretation and expert judgment. The classifications were performed by one experienced analyst, using a visualization scale between 1:500–1:1,000 and between 1:1,000–1:2,000, for the orthophotos and the Planet images respectively. In the orthophotos, it was possible to divide vegetation in three subclasses: sporadic, low (dominantly shrubby and herbaceous) and high (dominantly arboreal) vegetation. The spatial resolution of the Planet images instead allowed discrimination only between low and high vegetation.

The S2 images were automatically classified using a fuzzy convolutional neural network (CNN) algorithm on the four bands natively acquired at 10 m resolution (B2, B3, B4, and B8). The model predicts the fuzzy class membership of the water, dry sediment and vegetation classes. Neural networks are inherently fuzzy classifiers, terminating in a layer that has as many nodes as classes in the label data with assigned a likelihood of class membership (between 0 and 100). Fuzzy classification can thus infer sub-pixel scale compositions, and it has been seen as a way to mitigate for the relative coarse spatial resolution of the S2 images (Carbonneau et al., 2020). The CNN algorithm (see a full description in Carbonneau et al., 2020) was trained with a data set of high resolution (10 cm), multi-temporal unpiloted aerial vehicles (UAVs) images (5.25 km^2 of survey) which also included data from the study reach used here. For each 10 m S2 pixel, this UAV data provides 10,000 pixels which allowed for accurate estimation of the cover percentage of water, sediment and vegetation within each S2 pixel. The comparison between S2 and UAV data showed that the model predicted the fuzzy class memberships with median errors below 10% and mean absolute errors below 20%. This model is, to the best of our knowledge, the only fuzzy classification algorithm for Sentinel-2 imagery that is pre-trained for the Italian territory.

Once all images were manually (Planet and AGEA orthophotos) or automatically (S2) classified, we analyzed the results in terms of total area extent of water, sediment and vegetation. The fuzzy membership of each S2 pixel (expressed in percentage) was translated into semantic classes (where semantic refers to pixels labeled with a certain class name) according to the highest fuzzy membership of that pixel across the three classified classes. Given that the S2 images were classified only into one vegetation class (although with different degrees of fuzzy

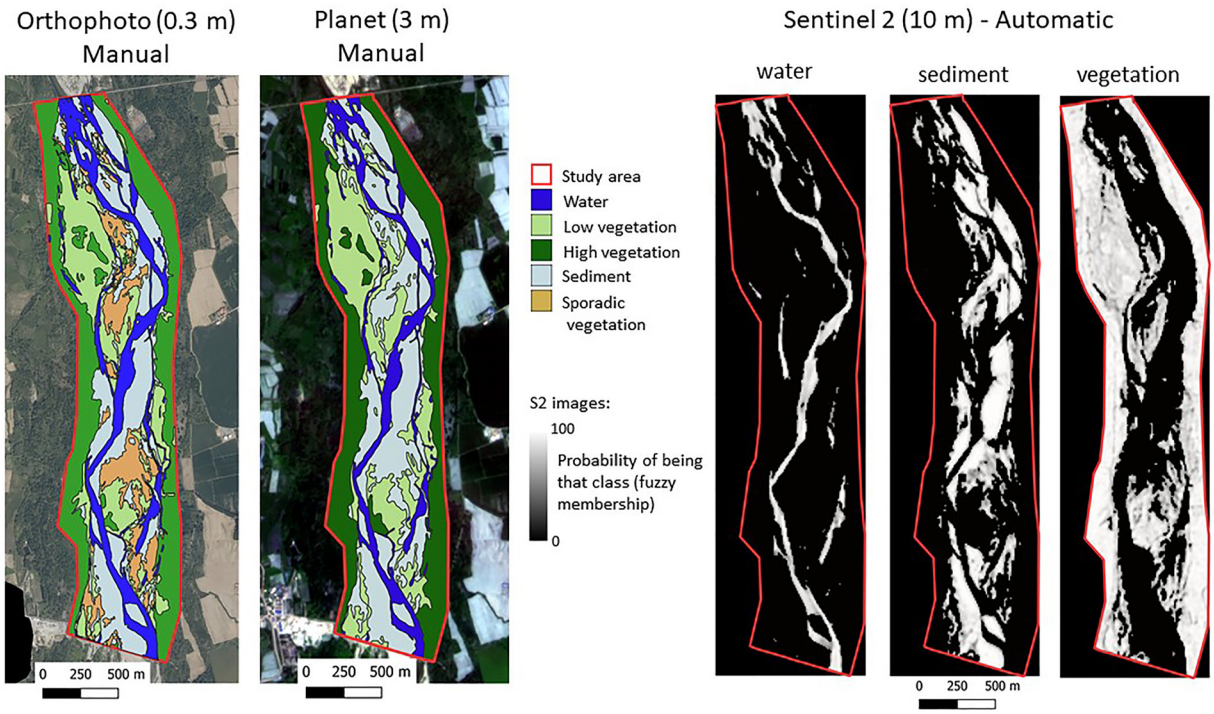

Figure 2. Example of the manual (orthophoto and planet images) and automatic (S2 images) classification performed for May 2022. For each analyzed date, the S2 pixels are assigned with a fuzzy membership of each class (from 0 to 100). The semantic class (label of water, sediment, and vegetation) is assigned according to the highest fuzzy membership of that pixel across the three classified classes.

membership), we lumped the vegetation subclasses of the orthophotos and of the Planet images also into one class, treating the different densities (e.g., sporadic) and the vegetation growth characteristics (high vs. low) as a useful side-information for the interpretation of the misclassification results. We approximated the classified orthophoto as error-free, recognizing that a digitization process driven by human interpretation will always present some spatial uncertainty. We then quantified the differences of the classes area extent between image sources using a normalized error (in hectares per square kilometers—hr/km^2), calculated as the ratio of the difference between the areas of the Planet or the S2 and the orthophoto (assumed the reference "ground-truth") divided by the area of that class obtained in the orthophoto.

To identify the nature of the misclassified pixels, we resampled the Planet and the S2 images to 0.3 m and we co-registered them with the orthophotos. In total, we obtained for all images 28,842,058 pixels of 0.3 × 0.3 m size (a total area equal to 2.6 km^2). In the pixel-by-pixel comparison, it was then possible to identify those pixels of the Planet and the S2 images that were classified as belonging in the same semantic class of the orthophotos (True Positive and True Negative) and those that were misclassified into different classes (False Positive and False negative). These correctly and misclassified pixels were reported in confusion matrices. The accuracy of the Planet- and S2-based classification was assessed as the ratio between the sum of the True Positives and Negatives of the three classes and the sum of both the True and False Negatives and Positives. The diagonal of the confusion matrix instead represents the precision of the classification, that is, the ratio between the True Positive and the sum of the True Positive and False Positive of each class.

In Figure 2, we show one example of the classified orthophoto, Planet and S2 images. As shown in the figure, sporadic vegetation is present only in the orthophoto. The CNN model generates for the S2 images three rasters, each one reporting the probability of belonging to the class of water, sediment and vegetation (the fuzzy membership between 0 and 100).

3.3. Temporal Evolution of the Geomorphic Features

We compared the temporal evolution of the three semantic classes across the three different temporal resolutions considered (orthophoto, Planet and S2 images). For this purpose, as mentioned in Section 3.1, beside

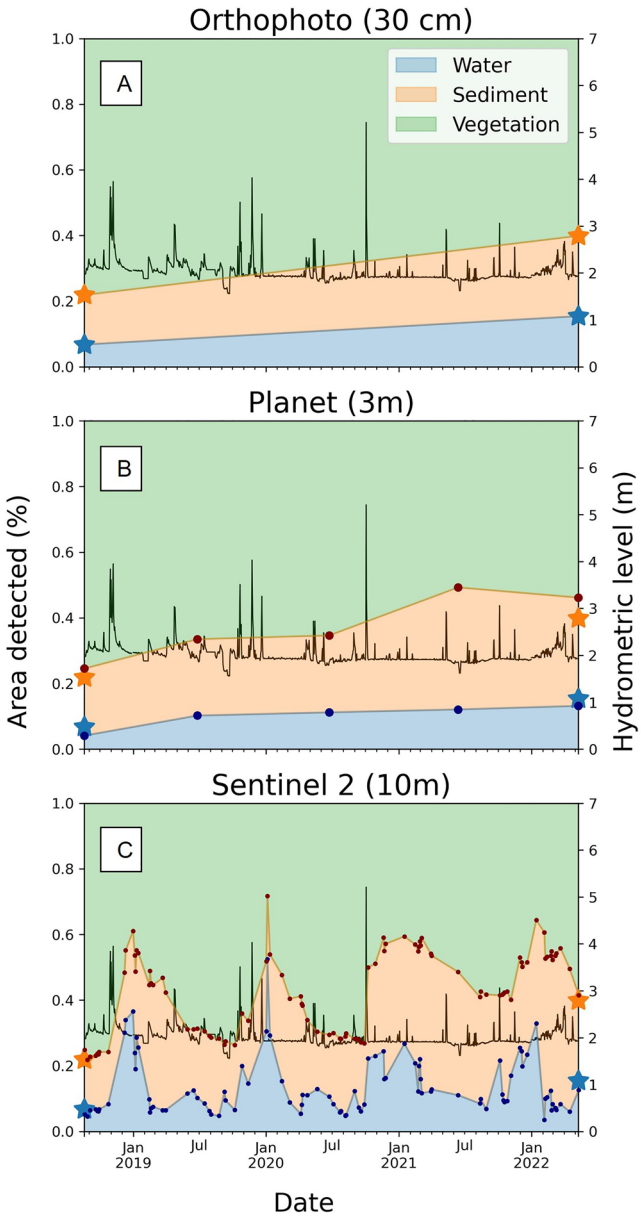

Figure 3. Classified percentage areas of the three semantic classes: water, sediment and vegetation. The star symbols in panel (a) identify the percentage of water (blue stars) and sediment (orange stars) classified in the AGEA orthophotos 2018 and 2022. The symbols are repeated also in panel b (Planet) and panel c (Sentinel 2) to facilitate the comparison. In the second axes, the hydrometric level (black line) recorded at the Palestro gauging station (see Figure 1).

the two available orthophotos available in the 5 years window (2018–2022), we downloaded one Planet image per year (five images in total) acquired in late spring or summer, and all the available S2 images (110 images in total). These images were manually (Planet images) or automatically (S2 images) classified as described above. We remind the reader, that the Planet images have higher spatial and temporal resolution than the S2, and their spatial uncertainty could be explored in similar ways to the one presented in this work for the S2. We selected the S2 images because they are freely available globally and because we already had an automatic S2 classifier tested on the study area (Carbonneau et al., 2020).

Finally, to better interpret the results, we considered the water hydrometric levels of the Sesia River available from the nearby Palestro gauging station (Figure 1) that allowed identification of floods and the alternance between dry and wet periods. This data was used to identify potential links between any severe hydrological event that occurred over the study period and temporal changes in the area extent of the classified semantic classes on the study site.

4. Results

4.1. Comparison Between the Three Spatial Resolutions

The first analysis considers the comparison between the spatial resolutions of the three image sources. The visual comparison in Figure 3 highlights that in both the Planet and the S2 the water is under classified when compared to the orthophoto (the star symbol is above the dot symbol), whereas the sediment percentage is over classified (the star symbol is below the dot symbol). These errors (which assume that the orthophoto is the "true" classification—see Section 3.2) are quantified in Table 2.

Table 2 shows that the water area calculated at resolutions lower than the orthophotos is underestimated by approximately 20% (up to 26% for the Planet in 2018). Sediments are consistently overestimated, with areas up to +35% (Planet 2018). Vegetation is instead under estimated (maximum −10% in the Planet 2022). By comparing the two image sources, the percentage error in the area extent results higher in the Planet images. These findings are partly unexpected, given that the Planet images have higher spatial resolutions than the S2 images. To better interpret these results, we visually compare the classified images and compute the confusion matrices.

Figures 4 and 5 compare the delineation of the three semantic classes at the three different resolutions.

Panels a–f in Figure 4 and panels a–b in Figure 5 highlight how water gets underestimated at lower spatial resolutions. In the Planet imagery, the manual classification underestimates the channel boundary delineation due to a combination of hanging vegetation (panels b in Figures 4 and 5), as well as to the presence of bank- and bed-sediments (panels b, e in Figure 4 and panels a, c in Figure 5). The same considerations hold for the S2 (panel d in Figure 5). The sediment class is consistently over-estimated in both the Planet and Sentinel images when compared to the orthophoto. Panels g–n in Figure 4 show that such an over estimation is mostly due to the misclassification of sporadic vegetation, a class present only in the orthophoto. The smaller overestimation of the sediment area in the S2 is associated with the use of an automatic model which recognizes low vegetation more consistently than the manual (color-based visual) delineation. As a consequence, the vegetation extent is more underestimated in the Planet than in the S2 images.

Table 2
Error Normalized With the Total Classified Area of That Class Within the Orthophoto (i.e., Within the Red Polygon of Figure 1)

	Water	Sediment	Vegetation
Error (hr/km^2) (*difference in hr*)			
Planet 2018	−26 (*−4.5*)	+35 (*+13.7*)	−4 (*−9.2*)
Planet 2022	−14 (*−5.9*)	+34 (*+22*)	−10 (*−16*)
Sentinel 2018	−22 (*−3.8*)	+29 (*+10.8*)	−3 (*−7*)
Sentinel 2022	−19 (*−7.3*)	+18 (*+11*)	−2 (*−3.7*)
Area (hr) (*relative %*)			
Orthophoto 2018	18 (*7%*)	40 (*15%*)	203 (*78%*)
Orthophoto 2022	40 (*15%*)	64 (*24%*)	156 (*60%*)

Note. If the error is negative there is an under-estimation of the total area compared to the orthophoto. If it is positive, there is instead an overestimation. The italic numbers represent the difference in hectares (h) between the areas derived from the classified Planet or S2 images and the orthophotos. The areas of the classes derived from the orthophotos are reported below in hectares (hr), together with the relative percentage of that class within the classified river corridor (Figures 1 and 2, red polygon).

By comparing Figures 4 and 5 with the errors reported in Table 2, we can deduce that the percentage error of the water class in the S2 might result smaller (e.g., 18% in 2018) than the error in the Planet (e.g., 26% in 2018) because of the coarser resolution of the S2 and not because the automatic classification outperformed the manual delineation. Panels C and F in Figure 4 and panel a in Figure 5 show for example, that the S2 have a greater water extent than the Planet but that the water pixels do not necessarily locate within the orthophoto boundaries. For the sediment class, the classification performed using the S2 is sometimes more conservative than in the Planet, with less sediment pixels classified at the expense of more sporadic vegetation (see the top left-hand side of panels h and i in Figure 4). However, in some cases the classification includes in the sediment class what was classified as vegetation in both the orthophoto and in the Planet (see right-hand side of panel I compared to panels g and h in Figure 4). Overall, the sediment area in the Planet results larger (with a higher overestimation—Table 2) but, as in the case of the water class, the pixels classified as sediment in the S2 often mismatch with those in the orthophotos (panel i compared to panel h in Figure 4).

Figure 6 quantifies this level of mismatch for all classes with a confusion matrix, which assesses the percentage of correctly and misclassified pixels. The values in the diagonal (darker color) represent the precision of the classification for each class. In general terms, (a) the Planet have a higher precision than the S2 and (b) the sediment classification has the lowest precision, with 20%–30% of the pixels misclassified at the expense of (sporadic) vegetation, as previously commented.

These results are in agreement with Figures 4 and 5, which show that the pixels classified as water in the Planet images are generally classified as water also in the orthophotos (thus the high precision in the two confusion matrices in Figure 6), with an underestimation due to a conservative water channel delineation. These considerations

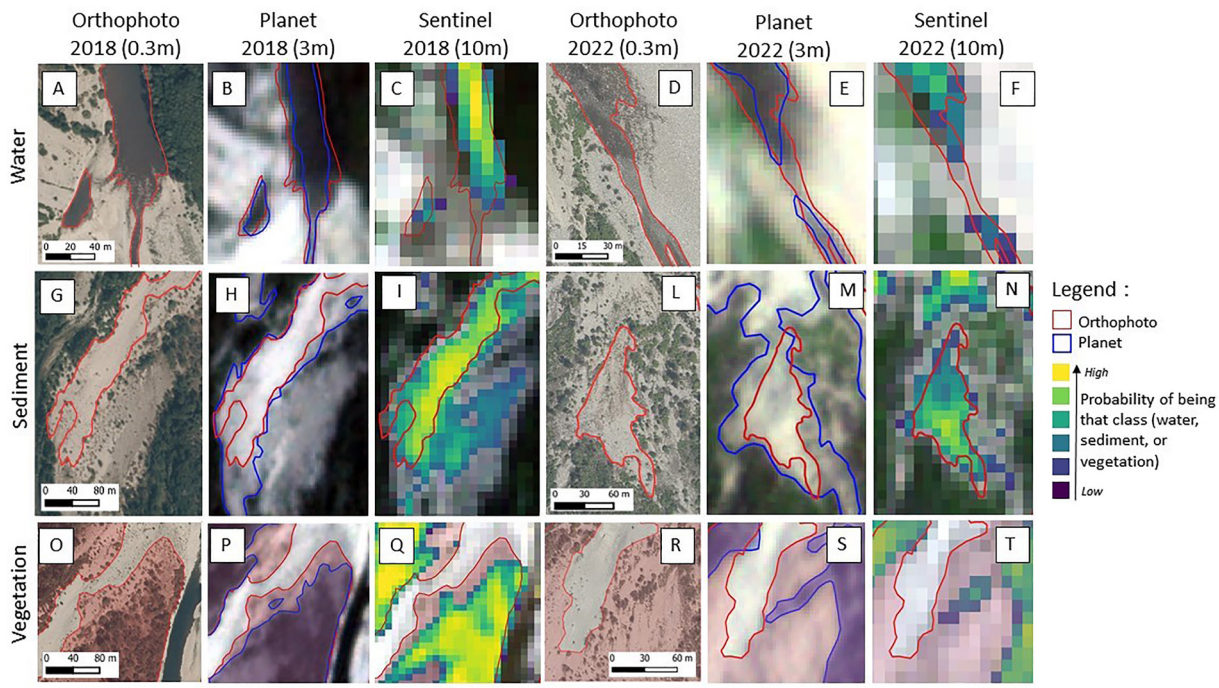

Figure 4. Examples of how the delineation of water, sediment and vegetation compare in the same location but at different resolutions and with different types of classification (manual in the orthophotos and Planet images; automatic in the S2 images). The figure highlights how water is underestimated at lower resolutions and how sediments instead are overestimated.

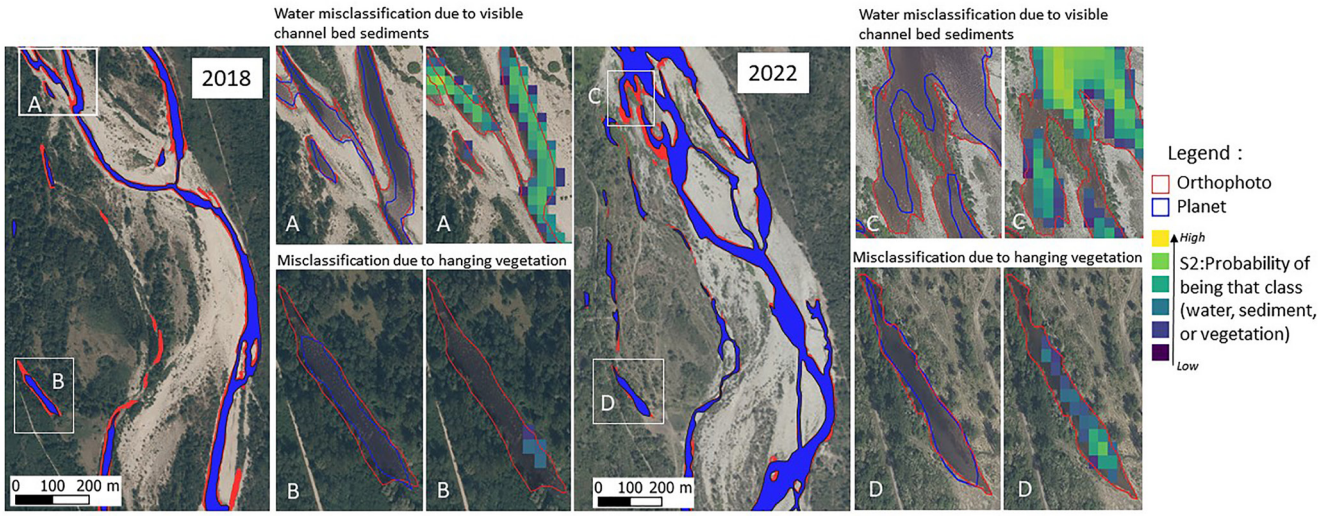

Figure 5. Difference in the classification of water on the same river section between the year 2018 (which includes panels a and b) and 2022 (which includes panels c and d). The figure also highlights the different river morphology before and after the flood event occurred in October 2020.

hold for the S2 images, although with a much greater level of misclassification in 2018: 26% of the water pixels were misclassified as sediment (19%) and vegetation (7%), compared to the 8% in 2022 (see the precision of the water class in Figure 6). The difference is due to the fact that in 2022 there is less (hanging) vegetation than in 2018 (see in Figure 5 the comparison between panels b and d) and the wetted branches of the multi-thread channel are wider and deeper (Figure 5). As a result, more water pixels are recognized by the automatic model within the water boundaries of the orthophoto and less pixels gets confused with visible bed sediments or vegetation. Therefore, even if the difference in the total areas with the orthophoto is higher in 2022 (as reported by the italics number in Table 2), the precision of the automatic model is higher (Figure 6) and the error percentage is smaller (Table 2).

4.2. Comparison Between the Three Temporal Resolutions

Figure 3 shows the fluvial geomorphic feature dynamics in terms of classified semantic classes in the three different temporal resolutions, providing different pictures of the river morphological change within the time window considered (2018–2022). From the two orthophotos (Figure 3a) and the five Planet images (Figure 3b), we could deduce that both the water and the sediment areal extent have increased throughout time. However, the comparison with the dense time series of the S2 reveals that such an increase might be associated with a temporary river channel configuration due to seasonal hydrometric conditions (see e.g., the increase in the water extent recorded in the Planet before 2020 and the corresponding water area extent in the S2 panel).

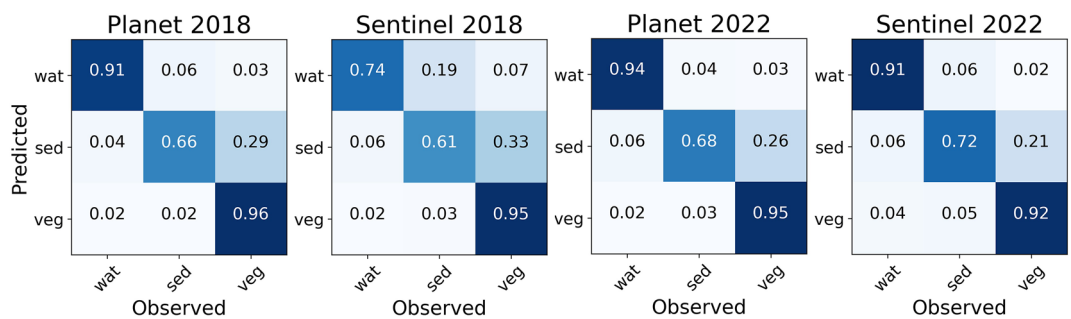

Figure 6. Normalized confusion matrices of the classified semantic classes (wat: water; sed: sediment; veg: vegetation). The normalized percentages are calculated by comparing the number of pixels of each class with the total pixels of that class in the orthophoto. In the first row of the left-hand side matrix for example, 91% of the pixels classified as water in the Planet 2018 were also classified as water in the orthophoto 2018; the remaining 6% and 3% of the pixels classified as water in the Planet 2018 (predicted) were classified respectively as sediment and vegetation in the orthophoto (observed).

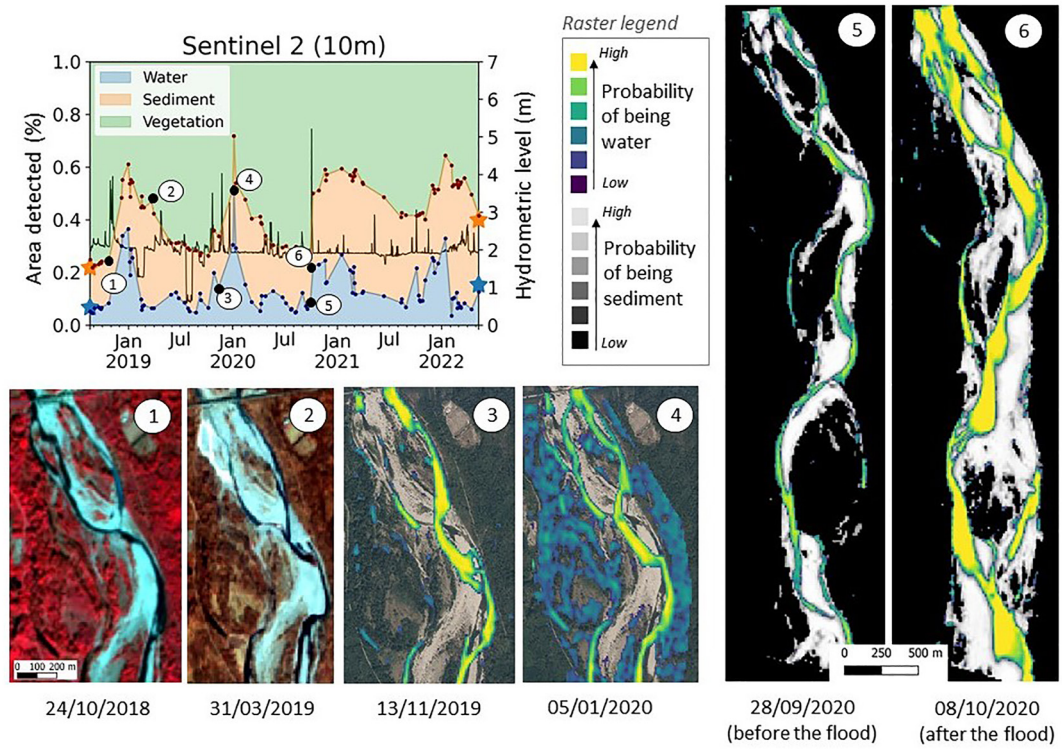

Figure 7. The top-left panel shows the temporal evolution of the classified area of the three semantic classes in the S2 images (same as in Figure 3). Each number reported in the graph is associated with the classified S2 image. In the raster legend, the probability of being a certain semantic class is represented by the fuzzy membership predicted by the automatic model.

To better interpret the morphological trends and potential outliers, Figure 7 links some of the water and sediment peaks found in Figure 3c with the associated S2 images. Peaks in the sediment area (where the difference between the sediment and the water area is greatest) generally occur after a water peak (see the peak two in Figure 7). After visual inspection within the time window considered, we deduced that the increase of sediment extents is mostly due to a combination of plant abscission during the winter season (see the comparison between panels 1 and 2 of Figure 7) as well as to high-water and sediment flows which locally remove or cover the vegetation on sediment bars, islands and floodplain (not shown). Peaks in the water area (see number 4 in Figure 7) occur together with, or soon after a registered high hydrometric level (black line in Figure 7). These peaks might sometimes include wet vegetation misclassified as water, potentially as a consequence of rainfall (see the comparison between panels 3 and 4 in Figure 7), or represent the consequences of flooding events. Panels 5 and 6 show for example, the change in the water and sediment areas before and after the major flood event of October 2020, with a substantial and almost instantaneous complementary decrease in vegetation cover (see top-left panel of Figure 7) as a response to the high-magnitude hydrological event.

In Figure 8 we compute the yearly median extent of water, sediment and vegetation to disentangle the seasonal morphological changes from the longer-term river evolutionary trajectories. Figure 8a shows how many times per year (i.e., yearly frequency), each pixel was classified as water or sediment. In 2021 (the year immediately after the major flood event of October 2020), both the water and the sediment area detected are visibly increased, for then decreasing in 2022. In Figure 8b, we quantified these yearly changes with boxplots for each semantic class. The bottom panel of Figure 8b confirms that the median water extent increased up to 2021, for then decreasing in 2022 with a recorded minimum in the time window considered. Similarly, the median sediment extent increased between 2018 and 2021, for then decreasing in 2022 with a complementary regrowth of the vegetation. However, the sediment median value of 2022 remains higher than in the previous years (as opposed to water), potentially indicating a more persistent river morphological change. Finally, Figure 8c shows the comparison of the active channel evolution discerned from the three image sources, assuming the active channel defined as the sum of the water and sediment areas (similar to Brousse et al., 2021; Gao et al., 2022; Ham & Church, 2002; Liébault

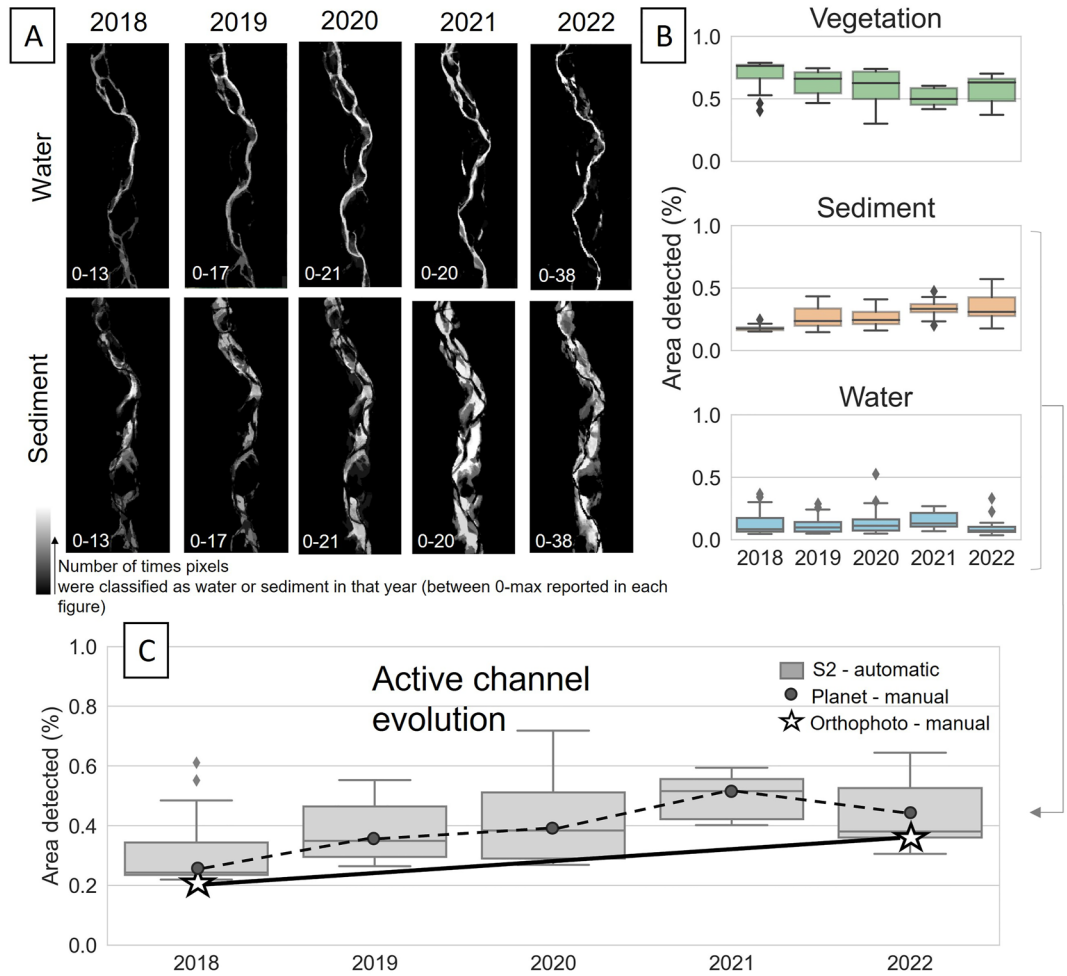

Figure 8. The top left-hand side (black and white) panel a show the yearly evolution of the water and sediment pixels resulting from the automatic classification of the S2 images. The whiter the pixel color, the higher the number of times that pixel was classified as water (top panels) or sediment (bottom panels). The legend is year-dependent and the minimum and maximum pixel values are reported in each panel. Panel b shows the box plots of the area percentage calculated within each year per each semantic class. Panel c shows the yearly active channel trajectory (assumed as the sum of the water and sediment pixels) assessed from the three image sources.

& Piégay, 2002). The plot shows that the Planet and the S2 trajectories are very similar, both detecting a sharper increase in the active channel extent in 2021 and a smoother decrease in 2022. When compared to the classification obtained from the two orthophotos (2018 and 2022), both trajectories overestimate the active channel area (between 5% and 15% if we consider the S2 median value) which is mostly due to an overestimation of the sediment extent as previously discussed. However, if only the two orthophotos were available in this time window, the geomorphic feature dynamics and in particular the ongoing decrease in the active channel extent recognized from Planet and S2 images would be masked by the low temporal resolution.

5. Discussion

5.1. The Impact of Different Spatial Resolutions on the Geomorphic Features Delineation

Table 2 and Figures 3 and 4 show that when we compare the S2 with the classification manually performed in the high resolution orthophotos, the water extent results underestimated of about 20% and the sediments extent overestimated of about 30%. As in previous studies, the number of water pixels is negatively influenced by overhanging vegetation (see panel b in Figure 5), shadows, and by shallow water columns which significantly modify the pixels reflectance contribution (panels a–f in Figure 4) (Güneralp et al., 2014; Pu et al., 2021).

Encroaching, sporadic vegetation instead did not have a sufficiently strong spectral signal to be classified as part of the vegetation class (even with low probability) rather than of the sediment class (e.g., as in Henshaw et al., 2013). These misclassifications are present in both the S2 and the Planet, with a relatively small difference between their normalized errors and the calculated area of the semantic classes (Table 2). While the smaller overestimation of the sediment area in the S2 (and a complementary underestimation of sporadic vegetation as previously commented—Table 2) is associated with the use of an automatic model which recognizes low vegetation more consistently than the manual delineation (Donovan et al., 2019), the similarity between the classified areas despite the jump in resolution (from 3 to 10 m) is unexpected. In a resampling exercise, Hollenhorst et al. (2006) showed that the proportional abundance of the classified riparian cover types remained preserved with spatial resolutions (from 5 to 90 m). The authors argued that the rate at which land covers types are lost at coarser resolutions is controlled by their clustering and not by the percentage in which they are present. The continuous linear nature of riverine wetlands and of the other riparian features might thus explain their findings. Here, we claim that the persistence of the classified areas under different resolutions is likely due to a combination of feature clustering (in this case: water, vegetation and sediment) and pixel size. As soon as the fluvial geomorphic feature is detectable (i.e., is larger than the pixel size), the accuracy of its delineation decreases with resolution but the area of its classified pixels increases. As a result, the potential underestimation error in the area extent can be smoothed down (see e.g., the water area in the panels a–f in Figure 4). We could therefore assume that on images with spatial resolution >1 m there is a systematic under/overestimation of the semantic classes which might be regulated by a percentage (in this analysis 20% for the water class) that is resolution-independent. More of these analyses should be performed to verify this hypothesis and its transferability to other locations. If a robust percentage was found, it could be treated as an upper or lower uncertainty bound to use when uncertainty cannot be properly assessed.

Looking at the nature of the misclassified pixels, Figure 6 demonstrates that water is under-classified mostly at the expense of sediment, whereas sediments are overclassified mostly at the expense of (sporadic) vegetation. These water and sediment misclassifications are also present in the Planet which achieve higher, but not as different precisions than the S2 (Figure 6). Indeed, the overall accuracy were respectively 0.88 for the Planet and 0.87 for the S2, with the S2 less able to recognize the water class, but better performing in 2022 in detecting the sediment class. For the S2, the higher precision in the water class detection in 2022 (Figure 6) can be explained by the increased of the water area percentage (see Table 2) and the change in the river morphology that occurred after the flood of 2020. Between 2018 and 2022, part of the (hanging) vegetation disappeared (Figure 5, panels b–d), and the channel widths as well as the water depths increased making them more detectable at the S2 pixel size resolution (Figure 5). The higher precision on the sediment detection in 2022 (which increases the overall accuracy—Figure 6) can also be associated with the 2020 flood event, where part of the sporadic vegetation was replaced with bare land (Figure 5—panels b–d). The S2 precisions could partly be influenced by a lack of georeferentiation with the orthophoto and by a manual digitization error of the orthophoto itself (Donovan et al., 2019). While the georeferentiation error is not quantifiable without ground-truth references, the manual digitization error could be assessed performing multiple digitizations of the same image. Previous studies that performed such analysis showed that the manual digitization error generally ranges between ±0.5 and ±5 m on images with resolutions between 0.2 and 1 m (Brenna et al., 2023; Donovan et al., 2019; Pu et al., 2021). While including an estimate of this error could increase the accuracy of our results, we argue that the persistent negative bias found in the water class (or positive bias in the sediment class) would remain on average negative (or positive) with the attribution of an ± "x" m error. Furthermore, a visual inspection of our results (see Figure 4) shows that the delineation errors between, for example, the manually classified orthophoto and the Planet images cannot be considered dominated by the inconsistencies of the analyst's digitization of the orthophoto; these errors (which can be random, or biased by the user's background) appear instead to be a small percentage of the error associated with mixed pixels in the Planet image - an error that is intrinsic to the Planet coarser resolution and not to the user ability to correctly distinguish the semantic class.

In general, the multi-spatial comparison performed in this work shows that similar accuracies and percentage errors can be found between resolutions. With these results, we can deduce that: (a) when the semantic classes are detectable, the correct delineation of spectrally mixed features (such as sediments and shallow water) remains challenging for both the manual and the automatic classification, at least for spatial resolutions >1 m (Hollenhorst et al., 2006; Ling et al., 2019; Rivas Casado et al., 2016); (b) classification performances can vary annually or inter-annually because of the hydrological history (Gleason et al., 2014; Hollenhorst et al., 2006; Werbylo et al., 2017); (c) the small difference in area detected and classification accuracy between the S2 and the Planet

images also provide evidence that automatic classifications are mature enough to substitute manual ones. This is pivotal, since manual classification cannot be carried out on a high number of images such as those available nowadays with satellites.

5.2. The Impact of Different Temporal Resolutions on the Interpretation of Fluvial Geomorphic Feature Dynamics

We analyzed the semantic classes dynamics under the three different temporal resolutions employed. Figures 3 and 7 show that the S2 provides a more detailed representation of the geomorphic features evolution, capturing those seasonal (panels 1–2 in Figure 7) as well as abrupt (panels 5–6 in Figure 7) river changes that are not detectable considering one (or less) image per year (as for the Planet images and orthophotos). For example, after the major flood of October 2020 there is an evident sudden increase of the water and sediment area (panels 5–6 in Figure 7). In the months that follow (i.e., March–November 2021), the vegetation quickly recolonizes the exposed sediment surfaces (e.g., bars) created by the flood (Figure 3c). These "instantaneous" or rapid changes are lost at lower temporal resolutions (Figures 3a and 3b) but represent an useful information for the understanding of the river dynamics and their drivers. Abrupt active channel widenings induced by infrequent high-magnitude floods (e.g., Rinaldi et al., 2016) and the following post-flood narrowing can occur over decadal (Friedman et al., 1996a, 1996b; Scorpio & Piégay, 2021), down to seasonal time scales if the environmental conditions (e.g., temperate and tropical climates) promote a high vegetation growth rate (Friedman & Lee, 2002). Images at low temporal resolution might not capture these transient morphological changes that compensate in between image acquisitions (Piégay et al., 2020). These reasonings suggest that for the study of rapid to instantaneous fluvial changes, in the absence of very high-resolution images acquired ad hoc, it is more informative to use lower spatial resolution data with higher temporal resolution such as S2 images than sporadic orthophotos. Having said that, temporary but erroneous configurations might also be recorded in the S2 because of variations of the model's performance throughout the year, for example, identifying temporary peaks in the water area because of the ambiguity between the spectral signal of wet vegetation and water (see panel 4 in Figure 7). In this case, the adopted CNN classification model (Carbonneau et al., 2020) was trained using only spring to late summer images. To classify seasonal changes, it would be thus necessary to sample the training data using also the other seasons and potentially add extra geomorphic classes (such as wet vegetation) if appropriate.

Nevertheless, those episodic events become less relevant when we consider the median of the classified classes over the years. These medians (the horizontal gray lines in the box plots of Figure 8c) can be used to represent the active channel (sediment + water) trajectory automatically extracted from the S2 images, at the net of the temporary morphological configurations (such as seasonal changes or erroneous classifications). Figure 8c shows that this trend is fully comparable to the active channel trajectory manually delineated from the Planet. Both trajectories show a moderate increase of the active channel from 2018 to 2020, followed by a sharper increase between 2020 and 2021. The first moderate increase can reliably be associated to a recent increase of sediment availability as observed in other Italian rivers (e.g., Bollati et al., 2014; Brenna et al., 2021). The last sharp increase instead represents the river response to the October 2020 flood, which induced major morphological effects along the Sesia River (ARPA, 2020; De Petris et al., 2021). The slight decrease of the active channel observed between 2021 and 2022 in favor of a moderate increase of vegetation cover is in accordance with the aforementioned recolonization of the vegetation (Figure 3c) that rapidly occurred in the fluvial corridor after the flood. This temporal trajectory is not recognizable from the two orthophotos acquired at the beginning and at the end of the study period, showing only a moderate increase of the active channel from 2018 to 2022 (Figures 3 and 8). Ziliani and Surian (2012) working on longer time scales (i.e., the last two centuries) highlighted that "*increasing the temporal resolution of evolutionary trajectory is crucial for interpretation of channel adjustments and comprehension of their controls*". The results summarized in Figure 8 are in accordance with this statement and demonstrate that the S2-derived trajectories can provide an informative reconstruction of the active channel changes which can be reasonably explained in terms of river processes occurred over the last few years (e.g., floods, channel widening, vegetation re-encroachment), at the least for the spatial and temporal scales considered. On the contrary, the temporal resolution of the orthophotos is not adequate for this aim since they lose crucial information about morphological changes and river processes that occurred in between the two available acquisitions.

5.3. The Impact of Spatial Uncertainty on the Interpretation of the Active Channel Trajectory

By combining the spatial and temporal analyses, the S2-derived active channel trajectory can be assumed to be robust even without the comparison with the Planet-derived trajectory. In 2018 and 2022, the normalized error

percentage with the centimetric orthophotos was found around 10% or less, with the underestimated water class (around 20%) compensating the overestimated sediment class (around 30%) (Table 2). Figure 8c shows that the detected morphological changes occurred in the active channel over the analyzed 5 years are two to three folds higher than such a spatial error, allowing to safely interpret the trajectories generated. In case the changes reported were comparable to or smaller than the error, caution should be used in the interpretation of the trajectories.

In general, errors on the interpretation of a certain geomorphic process will depend on the ratio between the temporal and spatial resolution of the image employed and a combination of the river size, morphology and dynamicity. Specifically, the spatial error will be a function of the dimension and the complexity of the geomorphic features, whereas the temporal error will be a function of their rate of change (e.g., the measure of erosion and accretion that can be detected). We could therefore expect that spatial errors on S2-based classifications would decrease, and classification performances increase for rivers that are wider and more stable (e.g., single-thread) than the Sesia River. Spatial errors could instead be comparable or larger in similarly morphologically complex, dynamic rivers such as multi-threaded or anastomosing rivers, where the presence of mixed pixels is generally abundant due, for example, to the presence of wet sediment bars and shallow water depths which have similar spectral signatures and can therefore be misclassified (Rowland et al., 2016). For what concerns temporal errors, short-term intervals will be necessary on highly dynamic rivers to capture the episodic nature of channel migration and its transient states (Petts & Gurnell, 2005). However, awareness on the timescale dependence in process rate estimations is also needed (how short does the interval between image acquisition need to be for capturing a certain geomorphic process on a certain type of river?).

In this work, we demonstrated that the spatiotemporal resolution trade-off of S2 images might lead to an understanding on the behavior of the river system that is similar to what can be derived from yearly images at 3 m spatial resolution, or even to a greater understanding (such as the persistence of changes after the flood event) than what could be gained at centimetric, multi-year resolutions. The results of this analysis therefore would not support the investment of having higher spatial resolutions (at least between 3 and 10 m) at the expense of revisit time. More analyses of this type, across different types of river could give insights on the transferability of the spatial uncertainty boundaries found in this work as well as on the appropriate spatial and temporal resolution trade-off for supporting different geomorphic analyses (Piégay et al., 2020). Multi-spectral images at finer temporal and spatial resolutions are commercially available (the Planet images, e.g.,) and would likely increase the accuracy in identifying fluvial geomorphic features and their dynamics (Fisher et al., 2018; Ziliani & Surian, 2012). However, wide spatial coverage might result into prohibitive costs which could for example, affect the return of investment of the watershed management policy that employed them (Fisher et al., 2018). S2-based analyses with freely available global coverage have instead the potential to better quantify the landforms-reach-catchment morphodynamic relationship, as well as discriminate which process is common across locations or is instead site-specific (Brierley et al., 2013). It is therefore important to explore existing data more deeply, assessing which data source is appropriate for which geomorphic issue. Quantifying the advantages and limitations of S2 images (or other remote sensed images) is the starting point to translate this data into a tangible advance in river process understanding.

6. Conclusions

This work aimed to quantify the uncertainty around the area extent of the water, sediment and vegetation classes automatically delineated on S2 images (10 m resolution, 5 days revisit time), and to evaluate how such an uncertainty could influence the interpretation of the active channel (sediment + water) trajectory for the 5 years analyzed (2018–2022). With these aims, we compared the classified classes across different spatial and temporal resolutions: multi-year with 0.3 m resolution (orthophoto) and yearly with 3 m resolution (Planet images). Assuming the orthophotos as error-free, the comparison led to the following findings.

Both the S2- and the Planet-based classification underestimate the water class and overestimate the sediments class, presenting comparable area percentage errors despite the jump in resolution. We deduce that similar results could be found in other acquisition dates and resolutions (>1 m) because such a spatial uncertainty depends on a combination of pixel size and pixel clustering, as well as on the correct delineation of "spectrally mixed" pixels which remains challenging for both the manual and the automatic classification.

The S2- and Planet-derived yearly active channel trajectory are comparable, whereas airplane derived orthophotos available every few years overlook the ongoing geomorphic feature dynamics at the scale of investigation and miss the episodic "instantaneous" river changes due to their low temporal resolution.

When we combine the spatial and the temporal analyses, we find that the spatial uncertainty found in the S2 are smaller than the morphological changes detected within the time window analyzed. The S2-derived active channel trajectory can then be considered robust. The similarity of this trajectory with the trajectory manually-derived from the Planet images also provides evidence that automatic classifications are mature enough to substitute manual ones. The use of infrequent, high spatial resolution (cm) and resource demanding imagery remains crucial to assess spatial classification uncertainties to then properly interpret the accuracy of the geomorphic trajectories derived from high frequency satellite images such as S2 or others.

Conflict of Interest

The authors declare no conflicts of interest relevant to this study.

Data Availability Statement

The orthophoto of 2018 by AGEA (Agenzia per le erogazioni in agricoltura) is publicly available on the Geoportale of the Piedmont Region. The link for the download: https://www.geoportale.piemonte.it/geonetwork/srv/ita/catalog.search#/metadata/r_piemon:98fe6c87-2721-4193-a35a-5af883badce7; with link WMS: https://opengis.csi.it/mp/regp_agea_2018?service=WMTS&request=GetCapabilities. The orthophoto of 2022 and all the classified images used for the analysis can be found in Bozzolan and Brenna (2023) via https://doi.org/10.5281/zenodo.8298522. The Planet images were downloaded at https://www.planet.com/ (accessed on 19 August 2022), whereas the Sentinel Level-2A at https://scihub.copernicus.eu (accessed on 14 July 2022). The full description of the fuzzy CNN model architecture can be found in P. E. Carbonneau et al. (2020). The model weights and the python code used for the fuzzy classification of the S2 images (respectively "Capo_5_32_4bande.h5" and "UAV2SEN_FuzzyCNN_BigTif.py") are available in Carbonneau (2023), version 2.0 (https://doi.org/10.5281/zenodo.8244818) with MIT licence.

Acknowledgments
This work was partly funded by the fellowships "Sediment dynamics and evolutionary trajectory of the Po River" and "Monitoring and modelling of river geomorphic processes and sediment transport by remote sensing information" supported by the University of Padova (DOR funds) and by the Autorità di bacino distrettuale del fiume Po. We particularly thank Dr Tommaso Simonelli for the access to the hydrological and geospatial datasets of the Sesia River. We would also like to thank the Reviewers for taking the time and effort necessary to improve this manuscript. This work was undertaken as part of the "The geosciences for Sustainable Development" (CUP C93C23002690001).

References

ARPA (2020). Evento DEL 2-3 OTTOBRE 2020.

Bizzi, S., Piégay, H., Demarchi, L., Van de Bund, W., Weissteiner, C. J., & Gob, F. (2019). LiDAR-based fluvial remote sensing to assess 50–100-year human-driven channel changes at a regional level: The case of the Piedmont Region, Italy. *Earth Surface Processes and Landforms*, *44*(2), 471–489. https://doi.org/10.1002/esp.4509

Bollati, I. M., Pellegrini, L., Rinaldi, M., Duci, G., & Pelfini, M. (2014). Reach-scale morphological adjustments and stages of channel evolution: The case of the Trebbia River (northern Italy). *Geomorphology*, *221*, 176–186. https://doi.org/10.1016/j.geomorph.2014.06.007

Boothroyd, R. J., Williams, R. D., Hoey, T. B., Barrett, B., & Prasojo, O. A. (2021). Applications of Google Earth Engine in fluvial geomorphology for detecting river channel change. *WIREs Water*, *8*(1), e21496. https://doi.org/10.1002/wat2.1496

Bozzolan, E., & Brenna, A. (2023). Raw and classified images (orthophoto, planet and sentinel 2) of a river reach of the Sesia River, Italy (time window: 2018–2022) (Version 0) [Dataset]. Zenodo. https://doi.org/10.5281/zenodo.8298522

Brenna, A., Marchi, L., Borga, M., Zaramella, M., & Surian, N. (2023). What drives major channel widening in mountain rivers during floods? The role of debris floods during a high-magnitude event. *Geomorphology*, *430*, 108650. https://doi.org/10.1016/j.geomorph.2023.108650

Brenna, A., Surian, N., & Mao, L. (2021). Alteration of gravel-bed river morphodynamics in response to multiple anthropogenic disturbances: Insights from the sediment-starved Parma River (northern Italy). *Geomorphology*, *389*, 107845. https://doi.org/10.1016/j.geomorph.2021.107845

Brierley, G. J., & Fryirs, K. A. (2016). The use of evolutionary trajectories to guide 'moving targets' in the management of river futures: moving targets for river management. *River Research and Applications*, *32*(5), 823–835. https://doi.org/10.1002/rra.2930

Brierley, G. J., Fryirs, K., Cullum, C., Tadaki, M., Huang, H. Q., & Blue, B. (2013). Reading the landscape: Integrating the theory and practice of geomorphology to develop place-based understandings of river systems. *Progress in Physical Geography: Earth and Environment*, *37*(5), 601–621. https://doi.org/10.1177/0309133313490007

Brierley, G. J., Reid, H., Fryirs, K., & Trahan, N. (2010). What are we monitoring and why? Using geomorphic principles to frame eco-hydrological assessments of river condition. *Science of the Total Environment*, *408*(9), 2025–2033. https://doi.org/10.1016/j.scitotenv.2010.01.038

Brousse, G. J., Liébault, F., Arnaud-Fassetta, G., Breilh, B., & Tacon, S. (2021). Gravel replenishment and active-channel widening for braided-river restoration: The case of the Upper Drac River (France). *Science of the Total Environment*, *766*, 142517. https://doi.org/10.1016/j.scitotenv.2020.142517

Carbonneau, P. E., (2023). PCdurham/UAV2Sen: UAV2SEN (Version 2.0) [Software]. Zenodo. https://doi.org/10.5281/zenodo.8244818

Carbonneau, P. E., Belletti, B., Micotti, M., Lastoria, B., Casaioli, M., Mariani, S., et al. (2020). UAV-based training for fully fuzzy classification of Sentinel-2 fluvial scenes. *Earth Surface Processes and Landforms*, *45*(13), 3120–3140. https://doi.org/10.1002/esp.4955

Carbonneau, P. E., Fonstad, M. A., Marcus, W. A., & Dugdale, S. J. (2012). Making riverscapes real. *Geomorphology*, *137*(1), 74–86. https://doi.org/10.1016/j.geomorph.2010.09.030

Dean, D. J., & Schmidt, J. C. (2013). The geomorphic effectiveness of a large flood on the Rio Grande in the Big Bend region: Insights on geomorphic controls and post-flood geomorphic response. *Geomorphology*, *201*, 183–198. https://doi.org/10.1016/j.geomorph.2013.06.020

De Petris, S., Sarvia, F., & Borgogno-Mondino, E. (2021). Multi-temporal mapping of flood damage to crops using sentinel-1 imagery: A case study of the Sesia River (October 2020). *Remote Sensing Letters*, *12*(5), 459–469. https://doi.org/10.1080/2150704X.2021.1890262

Donovan, M., Belmont, P., Notebaert, B., Coombs, T., Larson, P., & Souffront, M. (2019). Accounting for uncertainty in remotely-sensed measurements of river planform change. *Earth-Science Reviews*, *193*, 220–236. https://doi.org/10.1016/j.earscirev.2019.04.009

Fisher, J. R. B., Acosta, E. A., Dennedy-Frank, P. J., Kroeger, T., & Boucher, T. M. (2018). Impact of satellite imagery spatial resolution on land use classification accuracy and modeled water quality. *Remote Sensing in Ecology and Conservation*, *4*(2), 137–149. https://doi.org/10.1002/rse2.61

Friedman, J. M., & Lee, V. J. (2002). Extreme floods, channel change, and riparian forests along ephemeral streams. *Ecological Monographs*, *72*(3), 409–425. https://doi.org/10.1890/0012-9615(2002)072[0409:EFCCAR]2.0.CO;2

Friedman, J. M., Osterkamp, W. R., & Lewis, W. M. (1996a). The role of vegetation and bed-level fluctuations in the process of channel narrowing. *Geomorphology*, *14*(4), 341–351. https://doi.org/10.1016/0169-555X(95)00047-9

Friedman, J. M., Osterkamp, W. R., & Lewis, W. M. (1996b). Channel narrowing and vegetation development following a great plains flood. *Ecology*, *77*(7), 2167–2181. https://doi.org/10.2307/2265710

Gao, P., Li, Z., You, Y., Zhou, Y., & Piégay, H. (2022). Assessing functional characteristics of a braided river in the Qinghai-Tibet Plateau, China. *Geomorphology*, *403*, 108180. https://doi.org/10.1016/j.geomorph.2022.108180

Gilvear, D., & Bryant, R. (2016). Analysis of remotely sensed data for fluvial geomorphology and river science. In G. M. Kondolf & H. Piégay (Eds.), *Tools in Fluvial Geomorphology* (pp. 103–132). Wiley. https://doi.org/10.1002/9781118648551.ch6

Gleason, C. J., Smith, L. C., & Lee, J. (2014). Retrieval of river discharge solely from satellite imagery and at-many-stations hydraulic geometry: Sensitivity to river form and optimization parameters. *Water Resources Research*, *50*(12), 9604–9619. https://doi.org/10.1002/2014WR016109

Grabowski, R. C., Surian, N., & Gurnell, A. M. (2014). Characterizing geomorphological change to support sustainable river restoration and management: Characterizing geomorphological change in rivers. *Wiley Interdisciplinary Reviews: Water*, *1*(5), 483–512. https://doi.org/10.1002/wat2.1037

Güneralp, İ., Filippi, A. M., & Hales, B. (2014). Influence of river channel morphology and bank characteristics on water surface boundary delineation using high-resolution passive remote sensing and template matching: River water delineation using remote sensing and template matching. *Earth Surface Processes Landforms*, *39*(7), 977–986. https://doi.org/10.1002/esp.3560

Ham, D., & Church, M. (2002). *Channel island and active channel stability in the lower Fraser river gravel reach*. Department of Geography, University of British Columbia: Fraser River Research Group Report.

Harvey, J., & Gooseff, M. (2015). River corridor science: Hydrologic exchange and ecological consequences from bedforms to basins: River corridors from bedforms to basins. *Water Resources Research*, *51*(9), 6893–6922. https://doi.org/10.1002/2015WR017617

Henshaw, A. J., Gurnell, A. M., Bertoldi, W., & Drake, N. A. (2013). An assessment of the degree to which Landsat TM data can support the assessment of fluvial dynamics, as revealed by changes in vegetation extent and channel position, along a large river. *Geomorphology*, *202*, 74–85. https://doi.org/10.1016/j.geomorph.2013.01.011

Hollenhorst, T. P., Host, G. E., & Johnson, L. B. (2006). Scaling issues in mapping riparian zones with remote sensing data: Quantifying errors and sources of uncertainty. In J. Wu, K. B. Jones, H. Li, & O. L. Loucks (Eds.), *Scaling and uncertainty analysis in ecology* (pp. 275–295). Springer Netherlands. https://doi.org/10.1007/1-4020-4663-4_15

Kondolf, G. M., Piégay, H., & Landon, N. (2007). Changes in the riparian zone of the lower Eygues River, France, since 1830. *Landscape Ecology*, *22*(3), 367–384. https://doi.org/10.1007/s10980-006-9033-y

Liébault, F., & Piégay, H. (2002). Causes of 20th century channel narrowing in mountain and piedmont rivers of southeastern France: Causes of channel narrowing in SE France. *Earth Surface Processes Landforms*, *27*(4), 425–444. https://doi.org/10.1002/esp.328

Ling, F., Boyd, D., Ge, Y., Foody, G. M., Li, X., Wang, L., et al. (2019). Measuring River wetted width from remotely sensed imagery at the subpixel scale with a deep convolutional neural network. *Water Resources Research*, *55*(7), 5631–5649. https://doi.org/10.1029/2018WR024136

Petts, G. E., & Gurnell, A. M. (2005). Dams and geomorphology: Research progress and future directions. *Geomorphology*, *71*(1–2), 27–47. https://doi.org/10.1016/j.geomorph.2004.02.015

Piégay, H., Arnaud, F., Belletti, B., Bertrand, M., Bizzi, S., Carbonneau, P., et al. (2020). Remotely sensed rivers in the Anthropocene: State of the art and prospects. *Earth Surface Processes Landforms*, *45*(1), 157–188. https://doi.org/10.1002/esp.4787

Pu, G., Quackenbush, L. J., & Stehman, S. V. (2021). Identifying factors that influence accuracy of riparian vegetation classification and river channel delineation mapped using 1 m data. *Remote Sensing*, *13*(22), 4645. https://doi.org/10.3390/rs13224645

Righini, M., & Surian, N. (2018). Remote sensing as a tool for analysing channel dynamics and geomorphic effects of floods. In A. Refice, A. D'Addabbo, & D. Capolongo (Eds.), *Flood monitoring through remote sensing, springer remote sensing/photogrammetry* (pp. 27–59). Springer International Publishing. https://doi.org/10.1007/978-3-319-63959-8_2

Rinaldi, M., Amponsah, W., Benvenuti, M., Borga, M., Comiti, F., Lucía, A., et al. (2016). An integrated approach for investigating geomorphic response to extreme events: Methodological framework and application to the October 2011 flood in the Magra River catchment, Italy: Integrated approach for investigating geomorphic response to floods. *Earth Surface Processes Landforms*, *41*(6), 835–846. https://doi.org/10.1002/esp.3902

Rinaldi, M., Belletti, B., Bussettini, M., Comiti, F., Golfieri, B., Lastoria, B., et al. (2017). New tools for the hydromorphological assessment and monitoring of European streams. *Journal of Environmental Management*, *202*, 363–378. https://doi.org/10.1016/j.jenvman.2016.11.036

Rivas Casado, M., Ballesteros Gonzalez, R., Wright, R., & Bellamy, P. (2016). Quantifying the effect of aerial imagery resolution in automated hydromorphological river characterisation. *Remote Sensing*, *8*, 650. https://doi.org/10.3390/rs8080650

Rowland, J. C., Shelef, E., Pope, P. A., Muss, J., Gangodagamage, C., Brumby, S. P., & Wilson, C. J. (2016). A morphology independent methodology for quantifying planview river change and characteristics from remotely sensed imagery. *Remote Sensing of Environment*, *184*, 212–228. https://doi.org/10.1016/j.rse.2016.07.005

Scorpio, V., & Piégay, H. (2021). Is afforestation a driver of change in Italian rivers within the Anthropocene era? *Catena*, *198*, 105031. https://doi.org/10.1016/j.catena.2020.105031

Stecca, G., Zolezzi, G., Hicks, D. M., & Surian, N. (2019). Reduced braiding of rivers in human-modified landscapes: Converging trajectories and diversity of causes. *Earth-Science Reviews*, *188*, 291–311. https://doi.org/10.1016/j.earscirev.2018.10.016

Tomsett, C., & Leyland, J. (2019). Remote sensing of river corridors: A review of current trends and future directions. *River Research and Applications*, *35*(7), 779–803. https://doi.org/10.1002/rra.3479

Werbylo, K. L., Farnsworth, J. M., Baasch, D. M., & Farrell, P. D. (2017). Investigating the accuracy of photointerpreted unvegetated channel widths in a braided river system: A Platte river case study. *Geomorphology*, *278*, 163–170. https://doi.org/10.1016/j.geomorph.2016.11.003

Ziliani, L., & Surian, N. (2012). Evolutionary trajectory of channel morphology and controlling factors in a large gravel-bed river. *Geomorphology*, *173–174*, 104–117. https://doi.org/10.1016/j.geomorph.2012.06.001